DOI: 10.1002/ejic.200701297

Oxidative Ligand Rearrangement Due to Incipient Aminyl Radicals in the Oxidation of Iron(II) Species with Dioxygen

Remle Çelenligil-Çetin,[a] Patrina Paraskevopoulou,[b] Rupam Dinda,[b] Nikolia Lalioti,[c] Yiannis Sanakis,[d] Abdel Monem Rawashdeh,[b] Richard J. Staples,[e] Ekkehard Sinn,[b] and Pericles Stavropoulos*[b]

Keywords: Iron / N ligands / Radicals / Rearrangement / Tripodal ligands

The ferrous complex $[(L^1)Fe^{II}–THF]^-$, featuring the trisamido-amine ligand $[(RNC_6H_4)_3N]^{3-}$, where R is the electron-rich 4-*t*Bu-Ph moiety, can undergo a one-electron oxidation by dioxygen to afford the corresponding $[(L^1)Fe^{III}–OH]^-$ complex, and a parallel two-electron oxidation to generate the antiferromagnetically coupled diferric μ-oxo compound $[(L^1{}_{re-1})Fe–O–Fe(L^1{}_{re-1})]$. The latter compound possesses a ligand that exhibits oxidative rearrangement and retention of the oxidation equivalent in a *o*-diiminobenzosemiquinato moiety as a π radical. Ligand oxidation is perceived to initiate at an amido residue leading to formation of an electrophilic, metal-bould aminyl radical that undergoes an 1,4-(N-to-N) aryl migration reaction.

Introduction

Among the biologically relevant metalloradical systems explored, most prominent are those containing oxygen/sulfur residues,[1,2] as these electron-rich entities can better stabilize radical sites. In contrast, nitrogen-containing[3] radical moieties, such as aminyl ($NR_2^{\cdot}$) or amine radical cations ($NR_3^{\cdot+}$), have only recently started receiving due attention.[1] These weakly nucleophilic free radicals can be generated by oxidation or homolytic bond cleavage, and upon protonation or metalation can be transformed to reactive electrophilic moieties.[4] The present study provides a rare synthetic example in which dioxygen itself furnishes the requisite oxidizing power to initiate simultaneous metal- and ligand-centered oxidation, the latter leading to ligand rearrangement due to the reactivity of incipient *N*-centered radicals.

Results and Discussion

With reference to Scheme 1, entry into the iron chemistry of the new trisamido-amine ligand $[2\text{-}N(R)H\text{-}C_6H_4]_3N$ (L^1H_3; R = 4-*t*Bu-Ph) is accomplished by ligand deprotonation followed by addition of anhydrous $FeCl_2$ to afford light green crystals of $[(L^1)Fe^{II}–THF][K(THF)_3]\cdot 0.5THF$ (**1**) (see Figure 1 and Table S1 in the Supporting Information).[5]

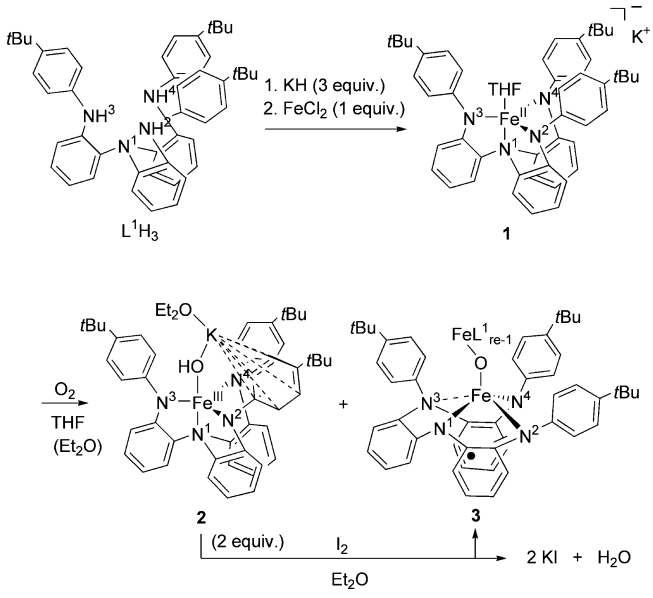

Scheme 1.

[a] Department of Chemistry, Boston University, Boston, MA, USA
[b] Department of Chemistry, University of Missouri-Rolla, 1870 Miner Circle, Rolla, MO 65409, USA
Fax: +1-573-341-6033
E-mail: pericles@mst.edu
[c] Department of Chemistry, University of Patras, Patras, Greece
[d] Institute of Materials Science, NCSR Demokritos, Ag. Paraskevi, Greece
[e] Department of Chemistry and Chemical Biology, Harvard University, Cambridge, MA, USA

Supporting information for this article is available on the WWW under http://www.eurjic.org or from the author.

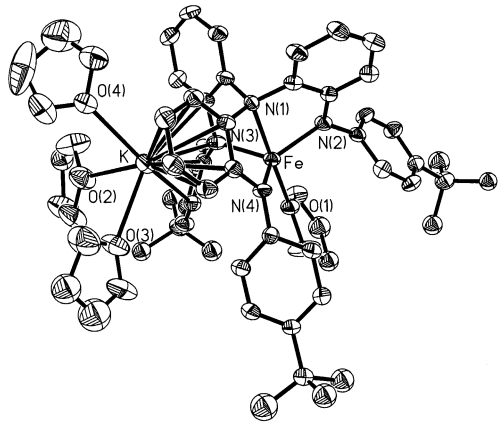

Figure 1. Solid-state structure of $[(L^1)Fe^{II}–THF][K(THF)_3]\cdot 0.5THF$ (**1**) showing 30% probability ellipsoids and the atom labeling scheme. Selected interatomic distances [Å] and angles [°]: Fe–N(2) 2.012(5), Fe–N(3) 2.055(5), Fe–N(4) 2.022(5), Fe–N(1) 2.266(5), Fe–O(1) 2.189(4), N(4)–Fe–N(3) 110.28(19), N(4)–Fe–N(2) 115.7(2), N(3)–Fe–N(2) 123.22(19), N(4)–Fe–O(1) 104.85(18), N(3)–Fe–O(1) 99.57(17), N(2)–Fe–O(1) 99.06(17), N(4)–Fe–N(1) 79.78(18), N(3)–Fe–N(1) 77.94(18), N(2)–Fe–N(1) 79.26(17), O(1)–Fe–N(1) 175.33(17).

Solutions of **1** in THF turn instantaneously blue-black upon exposure to dry dioxygen. The major isolable product is the blue $[(L^1)Fe^{III}–O(H)–K(OEt_2)]$ (**2**), while the black $[(L^1{}_{re-1})Fe^{III}–O–Fe^{III}(L^1{}_{re-1})]$ (**3**) is formed as a secondary crystalline species. Compound **2** can also be cleanly transformed to **3** by oxidation with iodine according to the stoichiometry of Equation (1).

$$2\,[(L^1)Fe^{III}–O(H)–K(OEt_2)] + I_2 \rightarrow [(L^1{}_{re-1})Fe^{III}–O–Fe^{III}(L^1{}_{re-1})] + 2KI + H_2O \quad (1)$$

The structure of **2** (Figure 2, Table S1)[5] features a bridging Fe^{III}–OH–K^+ moiety as part of a five-membered ring that also involves the well-established[6] K^+-(η^6-arene) interaction. The assignment of the hydroxo unit is supported by an Fe–OH bond length of 1.892(2) Å,[7] and by an IR band at $\nu(^{16}O–H) = 3612\ cm^{-1}$ which shifts to $3602\ cm^{-1}$ in an $^{18}O_2$-labeling experiment (see Figure S1, Supporting Information).[5] The source of hydrogen in –OH, whether due to H-atom abstraction from THF or residual water, has remained inconclusive. A reaction of **1** with O_2 in $[D_8]$THF proved to be complicated due to potential fast exchange between –OH(D) and residual H(D)O. Further experimentation is under way to resolve this issue.

The structure of **3** (Figure 3, Table S1)[5,8] reveals an intriguing oxidative reorganization of the ligand, which amounts to a formal 1,4-(N^1-to-N^3) migration of a phenylene group (ring between atoms N^1 and N^4 in **1** and **2**, Scheme 1). The oxidizing equivalent that triggers this rearrangement is retained on the ligand in the form of a radical-bearing *o*-diiminobenzosemiquinonato moiety (*o*-disq$^-$; Scheme 2).[9] X-ray data (80 K) reveal a pattern of four long (1.41 Å) and two short (1.37 Å) C–C bond lengths for the ring bridging between atoms N^1 and N^2, and an average C–N bond length (1.35 Å) lying between a single and a double bond. The semi-imino nature of moieties N^1 and N^2 [as well as of N^5 and N^6 on the second iron] is further evidenced by means of their Fe–N bond lengths [av. 2.032(3) Å], which are significantly longer than those associated with the genuine amido residues [Fe(1)–N(4) 1.960(5), Fe(2)–N(8) 1.957(5) Å].

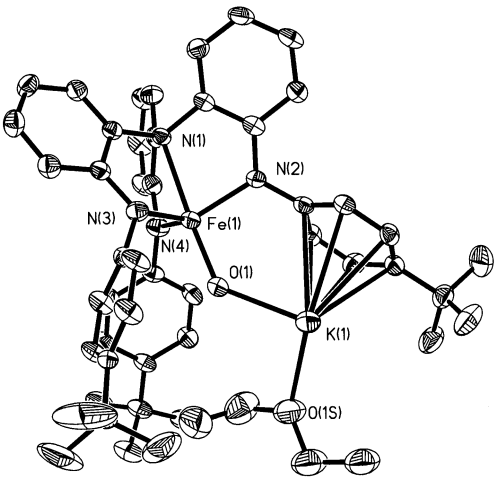

Figure 2. Solid-state structure of $[(L^1)Fe^{III}–O(H)–K(OEt_2)]$ (**2**) showing 50% probability ellipsoids and the atom labeling scheme. Selected interatomic distances [Å] and angles [°]: Fe(1)–O(1) 1.8923(19), Fe(1)–N(4) 1.952(2), Fe(1)–N(3) 1.967(2), Fe(1)–N(2) 2.000(2), Fe(1)–N(1) 2.314(2), K(1)–O(1) 2.515(2), K(1)–O(1S) 2.651(3), O(1)–H(1A) 0.9500, O(1)–Fe(1)–N(4) 105.71(9), O(1)–Fe(1)–N(3) 100.76(9), O(1)–Fe(1)–N(2) 100.03(9), O(1)–Fe(1)–N(1) 175.13(8), N(4)–Fe(1)–N(3) 111.29(9), N(4)–Fe(1)–N(2) 114.09(9), N(3)–Fe(1)–N(2) 121.82(9), N(4)–Fe(1)–N(1) 79.07(9), N(3)–Fe(1)–N(1) 78.03(9), N(2)–Fe(1)–N(1) 76.87(8), O(1)–K(1)–O(1S) 92.98(7), Fe(1)–O(1)–K(1) 134.55(10), Fe(1)–O(1)–H(1A) 112.7, K(1)–O(1)–H(1A) 112.7.

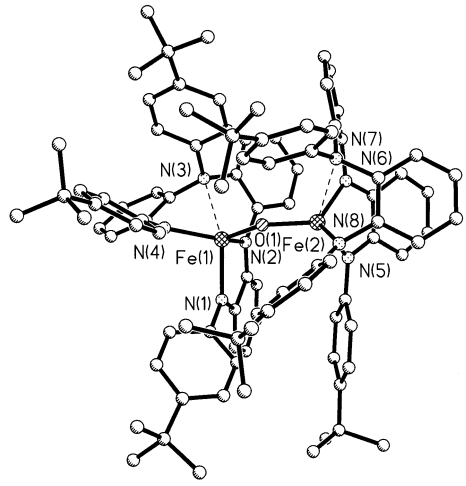

Figure 3. Solid-state structure of $[(L^1{}_{re-1})Fe^{III}–O–Fe^{III}(L^1{}_{re-1})]$ (**3**) showing the atom labeling scheme. Selected interatomic distances [Å] and angles [°]: Fe(1)–O(1) 1.772(4), Fe(2)–O(1) 1.786(4), Fe(1)–N(4) 1.960(5), Fe(1)–N(3) 2.458(4), Fe(1)–N(2) 2.023(4), Fe(1)–N(1) 2.037(5), Fe(2)–N(8) 1.957(5), Fe(2)–N(7) 2.487(4), Fe(2)–N(6) 2.017(5), Fe(2)–N(5) 2.051(4), O(1)–Fe(1)–N(4) 120.72(18), O(1)–Fe(1)–N(2) 107.29(18), Fe(1)–O(1)–Fe(2) 143.6(2), O(1)–Fe(1)–N(1) 111.73(19), N(2)–Fe(1)–N(1) 78.80(19).

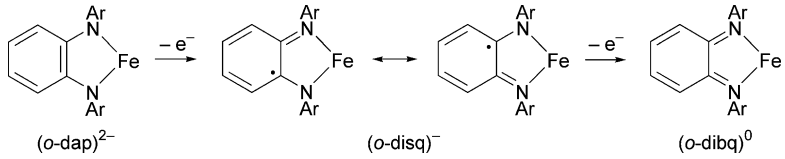

Scheme 2.

The ^{57}Fe Mössbauer effect of **3** at 90 K is consistent with the presence of an asymmetric, high-spin diferric site (δ = 0.363 ppm, 0.397 mm/s, ΔE_Q = 1.62, 1.47 mm/s, Γ = 0.45, 0.45 mm/s, Figure S2). The μ-oxo bridged unit displays an isotope sensitive ν(Fe–^{16}O–Fe) band at 830 cm^{-1} that shifts to 797 cm^{-1} upon use of $^{18}O_2$ in the oxidation of **1** (Figure S3).[5]

The best fit of the experimental molar susceptibility of **3** as a function of temperature (Figure 4, top) to the appropriate Hamiltonian[5] corresponds to $g_R = g_{Fe}$ = 2.0 (fixed), $J_{R-Fe} > -500$ cm^{-1} (undefined) for the strong antiferromagnetic coupling between Fe and the radical, and J_{Fe-Fe} = –125 cm^{-1} for the coupling between the two Fe^{III} centers,[8,10] along with an impurity of ρ = 8%. The non-zero susceptibility at low temperatures is due to paramagnetic impurities from high-spin ferric ions, which is also verified from the simulation of the magnetization data according to the Brillouin function (Figure 4, bottom).

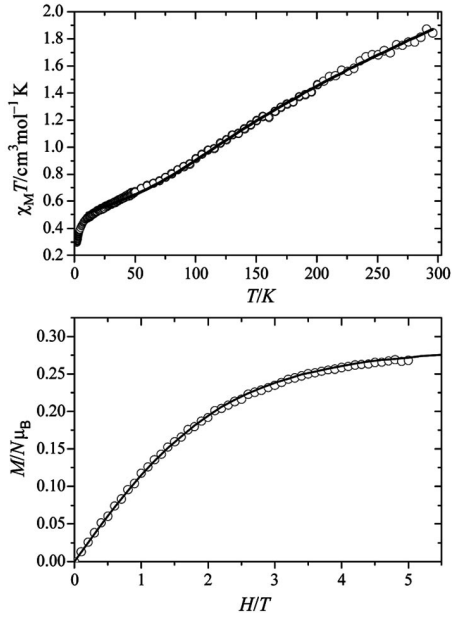

Figure 4. Top: temperature dependence of the susceptibility data of compound **3**, in the form of $\chi_M T$ vs. T (open circles) along with the fitting results (solid line). Bottom: magnetization data of compound **3** (open circles) along with a percentage (6%) of the theoretical Brillouin curve (solid line) of a paramagnetic ion with S = 5/2 and D = 0.33 cm^{-1}.

The X-band EPR spectrum of **2** in frozen toluene (3.2 K) shows an axial signal (g = 4.3), typical of high-spin ferric systems, along with a small impurity signal at g = 2.06, 2.00. The same signals are also present as impurities in the X-band EPR spectrum of **3** but with significantly different population in favor of the latter signal (Figure S4).[5]

Cyclic and differential pulse voltammograms of solutions of **3** in THF (Figure 5) exhibit remarkable redox chemistry, characterized by semi-reversible waves at $E_{1/2}$ values of –1.388 V (ΔE = 59 mV), –1.087 V (ΔE = 134 mV), –0.136 V (ΔE = 145 mV), 0.052 V (ΔE = 156 mV), and 0.258 V (ΔE = 131 mV) vs. the Fc$^+$/Fc couple. Other smaller features (the shoulder at –1.3 V and the small peak at –0.399 V) are attributed to impurities of **2** in **3**, as suggested by the vol-

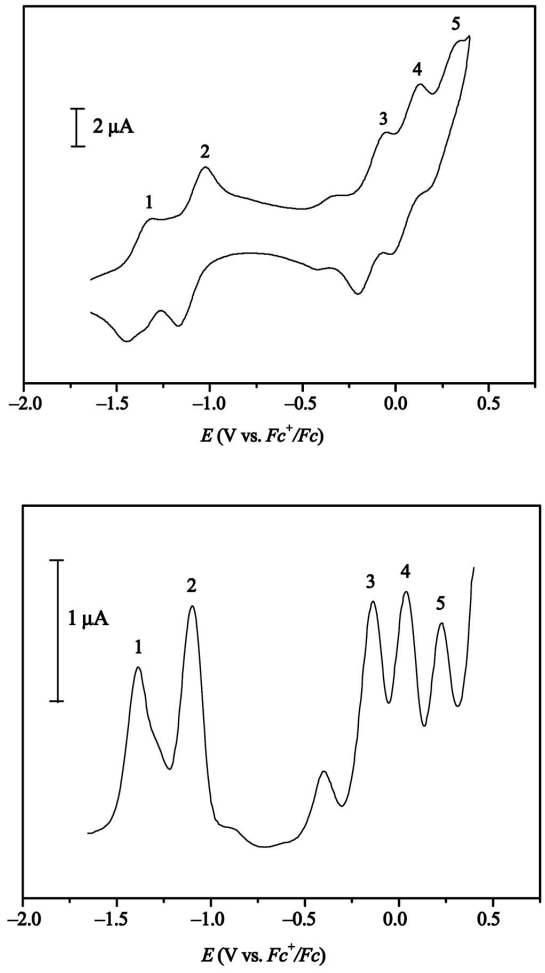

Figure 5. Cyclic (top) and differential pulse (bottom) voltammograms of **3** (3 mM) in THF/0.1 M [nBu$_4$N]PF$_6$ with a Au disk electrode (1.6 mm in diameter); scan rate 0.1 V/s (DPV: pulse width 100 ms; step time 2 s; pulse height 25 mV; potential increment 10 mV).

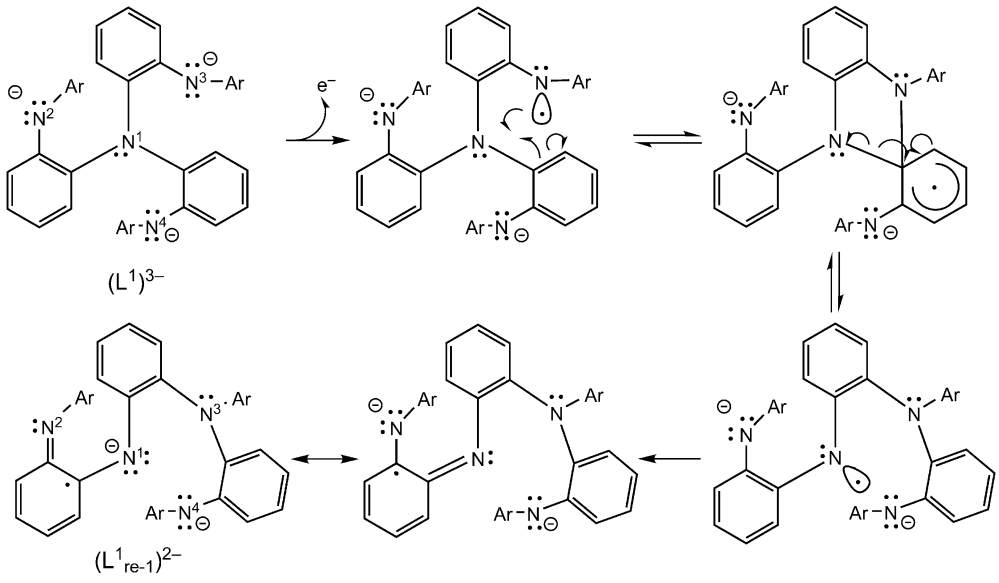

Scheme 3.

tammogram of **2** (Figure S5).[5] Conversely, the latter shows development of the characteristic waves of **3**, following an one-electron ligand-centered oxidation of **2**. Identification of the major single-electron events for **3** is in progress.

Cyclic and linear-sweep voltammetry experiments on **1** in THF show anodic/cathodic waves due to the Fe^{II}/Fe^{III} couple at very accessible potentials ($E_{1/2}$ = –1.264 V vs. Fc^+/Fc, ΔE = 103 mV, $i_{p,a}/i_{p,c}$ = 2.83; Figure S6)[5] followed by a two-electron anodic peak at $E_{p,a}$ = –0.382 V that is assigned to simultaneous oxidation of metal and ligand ($[(L^1)–Fe^{II}] \rightarrow [(L^1)^{\cdot}–Fe^{III}]$). Similar behavior is observed in DMF and DMSO, but importantly the anodic waves are shifted to more positive values by 344 and 319 mV, respectively. Consequently, the reaction of **1** with O_2 in these solvents only gives $[(L^1)–Fe^{III}–OH]^-$ and no ligand-based oxidation. Similarly, one-electron oxidation of the air-stable L^1H_3 is at $E_{p,a}$ = 0.325 V, whereas for the exceedingly air-sensitive K_3L^1 is at $E_{p,a}$ = –0.654 V (DMSO). These results suggest that the oxidation of **1** with O_2 takes place via two independent processes: a facile one-electron process leading to **2** and a more demanding two-electron process per [(L^1)–Fe] leading to **3**.

The electrochemical results and the calculated charge distribution data for L^1H_3 and the precursor tris(2-aminophenyl)amine at the DFT/B3LYP level of theory (Table S2),[5] strongly suggest that the protonated N_{amido} moieties are more electron-rich than the apical N_{amine} atom.[11] This is expected to be even more pronounced in compound **1**. The initial ligand oxidation here is also accompanied by metal oxidation and the resulting $R_2N^{\cdot}–Fe^{III}$ moiety features a reactive, electrophilic aminyl radical. Scheme 3 summarizes downstream steps toward the rearranged ligand (metal has been eliminated for clarity), chief among which is a radical 1,4-(N^1-to-N^3) phenyl migration,[12] which is well documented for carbon atoms and/or heteroatoms.[13]

This study exemplifies a rare case in which a metal-bound amido residue, which is vulnerable to one-electron oxidation by dioxygen, can trigger ligand rearrangement by generating an electrophilic aminyl radical that enables a radical 1,4(N-to-N) aryl migration and retention of the radical in a newly formed *o*-disq$^-$ moiety. Similar transformations may be central to other chemical and biological processes that split oxidation equivalents between the metal site and key residues.[14] Further studies will address whether this and other metalloradical systems can support higher metal valency.

CCDC-651014 (for **1**), -666573 (for **2**), and -666574 (for **3**) contain the supplementary crystallographic data for this paper. These data can be obtained free of charge from The Cambridge Crystallographic Data Centre via www.ccdc.cam.ac.uk/data_request/cif.

Supporting Information (see also the footnote on the first page of this article): Listings of experimental procedures, summary of the crystallographic data for **1**–**3** (Table S1), results from the DFT calculations (Table S2), FT-IR spectra of **2** and **3** (Figures S1, S3), Mössbauer spectrum of **3** (Figure S2), EPR spectra of **2** and **3** (Figure S4), cyclic voltammograms of **2** and **1** (Figures S5, S6).

Acknowledgments

This work was supported by the National Science Foundation (CHE-0412959) and in part by the National Institutes of Health (5 P42 ES007381). We thank Drs. N. Leventis, V. Tangoulis, J. Long, L. Berben and G. Long for useful discussions and experimental assistance.

[1] J. Stubbe, W. A. van der Donk, *Chem. Rev.* **1998**, *98*, 705–762.
[2] P. Chaudhuri, K. Wieghardt, *Prog. Inorg. Chem.* **2001**, *50*, 151–216.
[3] a) G. Merényi, J. Lind in *N-Centered Radicals* (Ed.: Z. Alsfassi), Wiley, New York, **1998**, pp. 599–613; b) B. J.

Maxwell, J. Tsanaktsidis in *N-Centered Radicals* (Ed.: Z. Alsfassi), Wiley, New York, **1998**, pp. 663–684.
[4] a) M. Newcomb, O. M. Musa, F. N. Martinez, J. H. Horner, *J. Am. Chem. Soc.* **1997**, *119*, 4569–4577; b) O. M. Musa, J. H. Horner, H. Shahin, M. Newcomb, *J. Am. Chem. Soc.* **1996**, *118*, 3862–3868; c) J. L. Esker, M. Newcomb, *Adv. Heterocycl. Chem.* **1993**, *58*, 1–45.
[5] See Supporting Information.
[6] a) J. C. Huffman, M. A. Green, S. L. Kaiser, K. G. Caulton, *J. Am. Chem. Soc.* **1985**, *107*, 5111–5115; b) M. W. Bouwkamp, E. Lobkovsky, P. J. Chirik, *Inorg. Chem.* **2006**, *45*, 2–4.
[7] a) R. Gupta, A. S. Borovik, *J. Am. Chem. Soc.* **2003**, *125*, 13234–13242; b) C. E. MacBeth, A. P. Golombek, V. G. Young Jr, C. Yang, K. Kuczera, M. P. Hendrich, A. S. Borovik, *Science* **2000**, *289*, 938–941.
[8] D. M. Kurtz Jr, *Chem. Rev.* **1990**, *90*, 585–606.
[9] a) D. Herebian, K. E. Wieghardt, F. Neese, *J. Am. Chem. Soc.* **2003**, *125*, 10997–11005; b) P. Chaudhuri, C. N. Verani, E. Bill, E. Bothe, T. Weyhermüller, K. Wieghardt, *J. Am. Chem. Soc.* **2001**, *123*, 2213–2223.
[10] S. Mukherjee, T. Weyhermüller, K. Wieghardt, P. Chaudhuri, *Dalton Trans.* **2003**, 3483–3485.
[11] F. G. Bordwell, X.-M. Zhang, J.-P. Cheng, *J. Org. Chem.* **1993**, *58*, 6410–6416.
[12] S. F. Wang, L. Mathew, J. Warkentin, *J. Am. Chem. Soc.* **1988**, *110*, 7235–7236.
[13] A. Studer, M. Bossart, *Tetrahedron* **2001**, *57*, 9649–9667.
[14] a) T. Büttner, J. Geier, G. Frison, J. Harmer, C. Calle, A. Schweiger, H. Schönberg, H. Grützmacher, *Science* **2005**, *307*, 235–238; b) A. Chanda, D.-L. Popescu, F. T. de Oliveira, E. L. Bominaar, A. D. Ryabov, E. Münck, T. J. Collins, *J. Inorg. Biochem.* **2006**, *100*, 606–619; c) J. W. Whittaker, *Arch. Biochem. Biophys.* **2005**, *433*, 227–239; d) C.-H. Wu, W. Jiang, C. Krebs, J. Stubbe, *Biochemistry* **2007**, *46*, 11577–11588.

Received: December 3, 2007
Published Online: January 7, 2008

